Mitochondrial protein import stress potentiates neurodegeneration in a mouse model of Parkinson's disease

Liam P. Coyne[1], Yumiko Umino[2], Xiaowen Wang[1], Eduado C. Solessio[2], Frank Middleton[3], & Xin Jie Chen[1,3]

1. Department of Biochemistry and Molecular Biology, State University of New York Upstate Medical University, Syracuse, NY 13210, USA.
2. Center for Vision Research, Department of Ophthalmology, State University of New York Upstate Medical University, Syracuse, NY 13210, USA
3. Department of Neuroscience and Physiology, State University of New York Upstate Medical University, Syracuse, NY 13210, USA.

Abstract

Mitochondrial biogenesis depends on the import of cytosolically synthesized proteins, and many pathophysiological conditions are expected to reduce protein import. However, despite severe mitochondrial protein import defects concomitant with impaired oxidative phosphorylation being implicated in ultra-rare neurodegenerative diseases, the neurological effects specific to protein import stress are unknown due to lack of an adequate animal model. Here, we fill this gap using our recently established protein import "clogger" mouse model, which expresses mutant adenine nucleotide translocase 1 (Ant1) that clogs the mitochondrial protein import machinery. While a small fraction of clogger mice undergo paralytic neurodegeneration, we show that non-paralytic mice do not have bioenergetic defects in the central nervous system. Non-paralytic clogger mice actually perform better than wild-type in behavioral assays of motor coordination and executive function. Transcriptomic analysis revealed signaling pathways directed towards counteracting proteotoxicity, possibly as a response to the accumulation of mitochondrial preproteins in the cytosol, a process known as mitochondrial Precursor Overaccumulation Stress (mPOS). IGF-2 was robustly upregulated in the spinal cord. IGF-2 is known to play a role in the extrusion of cytosolic protein aggregates into the extracellular space, in addition to its primary role in cell growth and development. To provide further support for a role of protein import stress in neurodegeneration, we crossed the clogger mice with a mouse model of Parkinson's disease expressing a cytosolic aggregation-prone protein, α-synuclein^{A53T}. We found that mild protein import stress significantly worsens motor coordination in α-synuclein^{A53T}, but not wild-type mice. In addition, double mutant mice showed modestly shortened maximal lifespan compared with α-synuclein^{A53T} animals. We found no evidence of impaired bioenergetics in the double mutant mice. These findings suggest that

mild protein import stress can modify neurodegeneration independent of bioenergetics. Future work is required to establish whether this occurs by enhancing cytosolic protein aggregation via mPOS.

Introduction

Mitochondrial defects and cytosolic protein aggregation in neurons are often co-manifested in neurodegenerative diseases such as Parkinson's disease (PD), Alzheimer's disease, Amyotrophic Lateral Sclerosis and Huntington's disease. These two hallmarks are shared despite significant variations in genetic and phenotypic makeup between diseases. Nevertheless, it is clear that both mitochondrial dysfunction and protein aggregation can individually drive neurodegeneration, but whether and how they interact during initiation and/or progression of these complex diseases is poorly understood, and likely to be multifactorial. The effects of pathogenic cytosolic protein species on mitochondrial function have been extensively investigated (*1*). By comparison, the mechanisms by which mitochondrial function affects cytosolic proteostasis and pathological protein aggregation is vastly understudied.

Recent work in yeast and human cells has shown that a wide range of mitochondrial stressors can reduce cell viability by reducing the import of mitochondrial preproteins causing their toxic accumulation and aggregation in the cytosol (*2-5*). This cell stress mechanism was termed mitochondrial Precursor Overaccumulation Stress (mPOS). In the context of neurodegeneration, this raises the intriguing possibility that mitochondrial dysfunction could directly contribute to cytosolic protein aggregation, thereby amplifying the effect of the proteostatic pathway of neurodegeneration. To our knowledge, this intuitive possibility has not been tested due to the lack of an adequate animal model of moderate protein import stress that does not severely affect oxidative phosphorylation. Such a model is critical for demonstrating the pathogenic effect specific to protein import defect and mPOS independent of bioenergetics.

Modeling mitochondrial protein import stress in animals is particularly challenging because virtually all mitochondrial functions depend on efficient import. All but 13 of the 1,000-

1,500 mitochondrial proteins are encoded in the nucleus, synthesized by cytosolic ribosomes and then imported into the organelle. The import machinery is intricate, relying on numerous chaperones both inside and outside mitochondria, as well as multiple pore-forming protein complexes in the inner and outer mitochondrial membranes (*6-8*). The entry gate for >90% of mitochondrial proteins is the translocase of the outer membrane (TOM) complex. We previously engineered mutant variants of the adenine nucleotide translocator that clog the TOM complex to obstruct general protein import (Coyne et al. 2022, *submitted*). The best-characterized clogger protein was $Ant1^{A114P,A123D}$, which we used to generate a mouse model. Approximately 4% of $Ant1^{A114P,A123D}$ /+ mice (or "clogger" mice) become paralyzed around 12 months of age, suggesting a direct role of protein import clogging in neurodegeneration. Yet ~96% of clogger mice have a normal lifespan, and do not develop overt neurological symptoms. In this study, we exploit these mice to study the specific effects of moderate protein import stress on neurological function. Most importantly, we then used mouse genetics to test whether moderate protein import clogging can accelerate neurodegeneration in a mouse model of Parkinson's disease that involves the misfolding and aggregation of the cytosolic protein, α-$synuclein^{A53T}$.

Results:

Mild protein import stress affects motor coordination and behavior but not memory in mice.

To explore the effects of protein import clogging on neurological function, we performed a battery of behavioral assays on non-paralytic clogger mice. To ensure validity of the behavioral assays, we first assessed vision and motor function. Using optomotor response testing, we confirmed that visual acuity and contrast sensitivity are preserved in clogger mice (Figure S1A-B). While 30-month-old clogger mice clearly exhibit skeletal muscle atrophy and weakness (Coyne et al., 2022, *submitted*), this effect appears age-dependent, as mice at the age of ~13 months have preserved muscle function, as suggested by treadmill exhaustion testing (Figure S1C-D). Swim speed to a visible escape platform was also unchanged in clogger mice (Figure S1E). We also tested ~20-month-old mice on an accelerating rotarod to measure motor coordination and balance. Surprisingly, we found that the clogger mice performed significantly better than wild-type mice, suggesting enhanced motor coordination and/or balance (Figure 1A).

To assess general locomotor activity, we performed an open field test. When left undisturbed in a brightly lit open field for 10 minutes, female clogger mice move at a faster average speed than wildtype (Figure 1B). This increased locomotor activity cannot be attributed to anxiety-like behavior, as suggested by clogger mice spending similar amounts of time in the "center zone" of the open field (Figure S2A). Rodents have a tendency to stay near the walls of a well-lit open field, a property known as thigmotaxis, and time spent away from the walls in the center zone is used as an index of anxiety in mice. Another test of anxiety-like behavior, the elevated plus maze, has two elevated walled arms perpendicular to two elevated open arms, and the amount of time spent in the open arms is similarly used as a proxy for anxiety-like behavior.

Clogger mice spent similar amounts of time in the open arms as wild-type, consistent with unaffected anxiety-like behavior (Figure S2B).

To assess cognitive function, we monitored animal behavior in a number of assays as a proxy for memory and executive function. The Y-maze spontaneous alternation test relies on rodents' natural tendency to explore new areas. When they repeatedly return to arms of the Y-maze that they were most recently in, this is interpreted as a defect in working spatial memory. This assay suggested that clogger mice have preserved working spatial memory (Figure S2C). The novel object recognition test relies on rodents' natural tendency to explore new objects after becoming familiarized with other objects over multiple prior training days. This assay suggested that clogger mice have preserved long-term recognition memory (Figure S2D). The Morris water maze tests rodents' ability to learn and remember the location of a hidden escape platform that they have to swim to, which is unpleasant for rodents. This assay suggested that clogger mice have preserved long-term spatial memory and learning (Figure S2E-G). Collectively, these data suggest that learning and memory are intact in clogger mice.

Finally, we tested executive function, which refers to higher-level cognition used to control and coordinate behavior. To test this, we used a "puzzle box" assay in which mice are placed in a stressful environment and the amount of time it takes to escape through an obstructed exit doorway is used as a proxy for executive function (*9*, *10*). We found that, for the most difficult obstruction ("Condition 4"), clogger mice were significantly better at escaping the stressful environment (Figure 1C). These data suggest clogger mice may have improved executive function that cannot be attributed to increased anxiety-like behavior, as shown above.

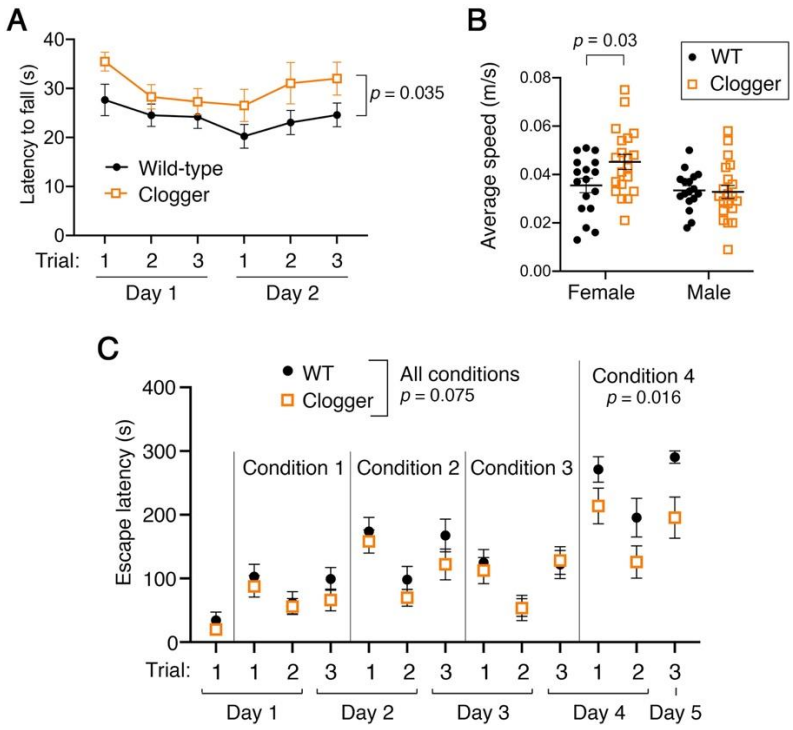

Figure 1. Mild protein import clogging positively affects motor coordination and executive function.

(A) Clogger mice ($Ant1^{A114P,A123D}$/+) perform better than wild-type on the accelerating rotarod. Mice aged 19-22 months (n > 16 mice per genotype, n > 5 per sex per genotype) were tested on a high-difficulty rotarod protocol of acceleration from 4 to 40 rpm over 2 minutes. Data were analyzed with a two-way repeated measures ANOVA probing for an effect of sex and genotype, with Geisser-Greenhouse correction. Depicted is the main-effect of genotype.

(B) Female clogger mice have increased spontaneous locomotor activity. Two independent aged mouse cohorts (14-17 months of age) were monitored in the open field apparatus and average speed throughout the 10 minutes was plotted. Data were analyzed with a two-way ANOVA with Sidak's multiple comparison's test. Each dot is an unique mouse.

(C) In the "puzzle box" assay, clogger mice are faster than wild-type in removing obstacles from a 5 cm x 5 cm doorway to escape from a stressful environment, suggesting enhanced executive function (20-23.5 months of age; n = 13 wild-type including 5 females and 8 males; n = 15 cloggers including 9 female and 6 male). Different "Conditions" are different obstacles. "All conditions" p-value was derived from a repeated measures ANOVA (with Geisser-Greenhouse correction) probing for an effect of genotype with the 13 repeated trials as the within-subjects variable. P-value from "Condition 4 only" derived the same way except with only condition 4 data.

Ant1$^{A114P,\ A123D}$-induced protein import clogging does not affect mitochondrial bioenergetics in the brain

Similar behavioral changes, including increased voluntary locomotor activity and performance on the rotarod, have been reported in mutant mice affected in mitochondrial function, which was speculated to be caused by bioenergetic function (*11*, *12*). We therefore wondered whether reduced mitochondrial bioenergetics contributes to the behavioral phenotypes in the Ant1^{A114P,A123D}/+ clogger mice. To test this, we measured oxygen consumption from purified brain mitochondria. Unlike skeletal muscle (Coyne et al., 2022, *submitted*), brain mitochondria from clogger mice do not have reduced maximal respiratory rate (state 3) when stimulating complex I (Figure 2A-B). ADP-depleted respiration (state 4) and the respiratory control ratio (state 3/state 4) were also unchanged (Figure 2C-D). These observations suggest mitochondrial oxygen consumption is well-coupled with ATP synthesis and the maximal complex I-based respiratory capacity is not reduced in clogger brain mitochondria. Mitochondrial respiration was also unaffected when complex I is inhibited with rotenone and complex II is stimulated with succinate (Figure 2E-H). Thus, mitochondrial respiration is unaffected or minimally affected in mouse brain. Consistent with this, we assessed the steady-state levels of respiratory chain proteins by immunoblot and found that representative subunits of complexes I, II, III and V were unaffected in clogger brain mitochondria (Figure 2I). Given that Ant1$^{A114P,\ A123D}$-induced protein import clogging alters motor function, we extended our analysis to the spinal cord by directly examining mitochondrial morphology using transmission electron microscopy. The data showed preserved mitochondrial morphology in ventral horn neurons in the non-paralytic clogger mouse spinal cord (Figure 2J). Taken together, these data suggest that

mitochondrial structure and function are generally preserved in the central nervous system of clogger mice.

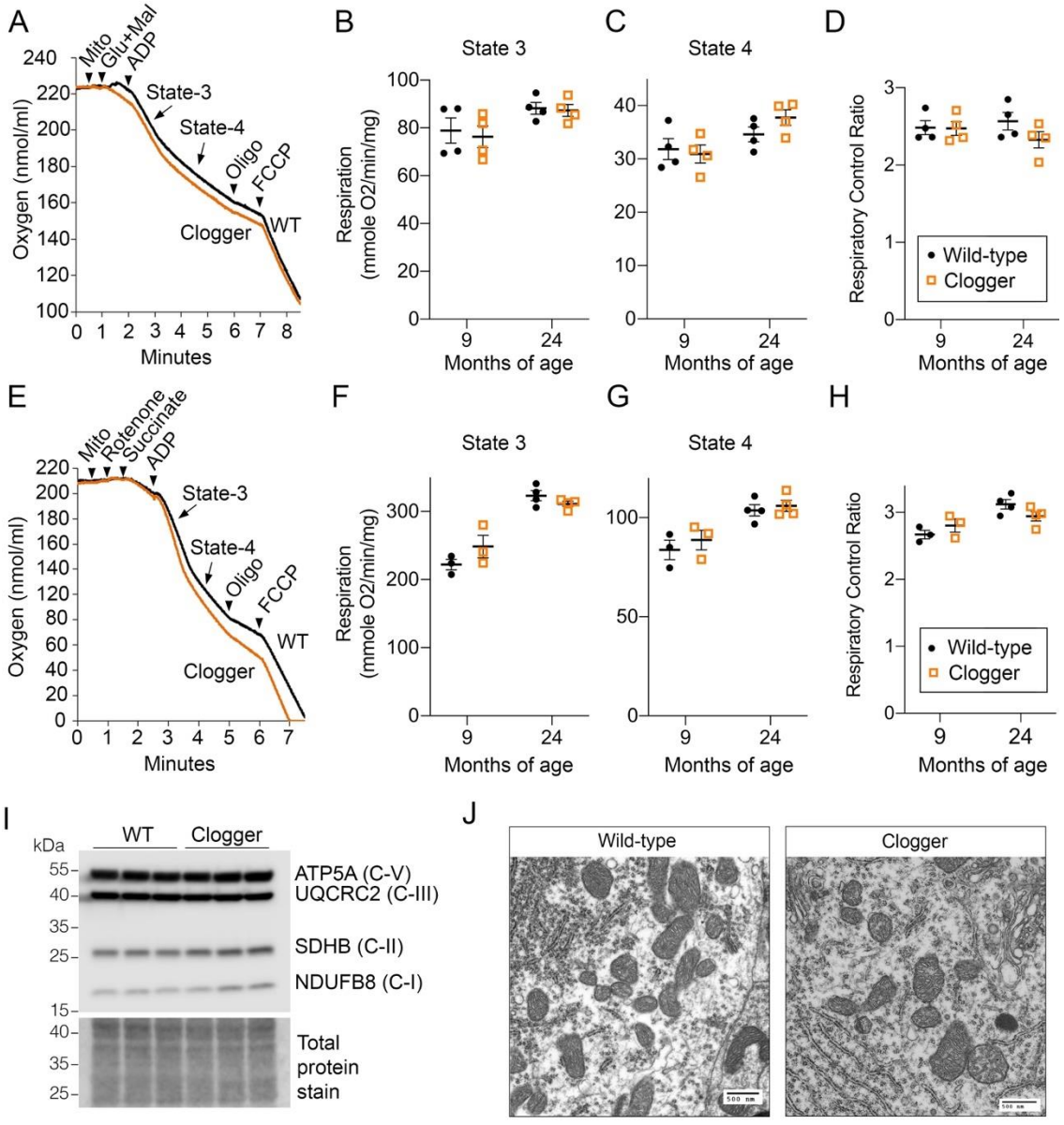

Figure 2. Mild protein import clogging does not affect mitochondrial bioenergetics in the central nervous system.

(A) – (D) Respirometry of purified brain mitochondria with complex I stimulated by glutamate (glu) and malate (mal). N = 4 mice/genotype/age group. 2 measurements were taken per mouse, the average of which is plotted in (B)-(D). Data from different ages were analyzed separately due to a suspected batch effect. Independent repeated measures

ANOVA within each age group (with measurement order as the within-subjects variable and genotype as the between-subjects variable) confirmed no effect of measurement order or genotype for any measure potted in (B)-(D) or (F)-(H). FCCP, Trifluoromethoxy carbonylcyanide phenylhydrazone; Oligo, oligomycin; Glu, glutamate; Mal, malate. State 3 respiration is the maximal respiratory rate after addition of ADP. State 4 respiration is the respiratory rate after depletion of ADP. The respiratory control ratio is State 3 divided by State 4 respiratory rates. Decreased respiratory control ratio would be interpreted as increased mitochondrial damage.

(E) – (H) Respirometry of purified brain mitochondria with complex II stimulated by succinate and complex I inhibited by rotenone. N = 3 mice/genotype at 9 months of age and 4 mice/genotype at 24 months of age. Data collected and analyzed as in (A)-(D).

(I) Immunoblot analysis of representative subunits of the respiratory complexes from purified brain mitochondria.

(J) Electron microscopic analysis in the cell body of spinal cord ventral horn neurons showing no obvious changes to mitochondrial ultrastructure in non-paralytic clogger mice. Scale bar is 500 nm.

Transcriptional remodeling in the central nervous system.

To learn whether Ant1$^{A114P,\ A123D}$-induced protein import clogging triggers specific stress responses, we first performed RNAseq analysis to the spinal cord because the spinal cord appears to be preferentially affected in the clogger mice (Coyne et al., 2022, *submitted*). We found a robust transcriptional signature of 149 differentially expressed genes ($q < 0.05$) (Figure 3A). Among the four most upregulated genes were *HSPA1B, IGF2* and *IGFBP6* (Figure 3B). *HSPA1B* codes for HSP70, a molecular chaperone that protects against protein aggregation and mediates folding of newly synthesized proteins. It is also involved in the stabilization and mitochondrial delivery of mitochondrial preproteins in the cytosol (*13*). This observation is consistent with the finding that *HSPA1B* is transcriptionally activated in HEK293T cells challenged by an import clogger protein (*5*), and that yeast HSP70 genes were upregulated upon clogging by Aac2^{A128P} (Coyne et al., 2022, *submitted*). The data are also in concordance with previous findings with a synthetic protein import clogger (*14*). We also previously found

increased physical association of HSP70 family members with Aac2^{A128P} (Coyne et al., 2022, *submitted*). Taken together, these data suggest that transcriptional upregulation of HSP70 genes is a common response to mitochondrial protein import clogging.

Insulin-like growth factor-binding proteins (IGFBPs) are secreted proteins that bind insulin-like growth factors (IGFs) to regulate their transportation, localization, and function. IGFBP-6 is unique to this family in that it has a 20- to 100-fold higher affinity for IGF2 compared with IGF1 (*15*). Thus, co-induction of IGFBP-6 and IGF2 in clogger-mouse spinal cords suggests activation of a coordinated stress response. Recent studies demonstrated that IGF2 can protect against neurodegeneration through extracellular disposal of protein aggregates (Garcia-Huerta et al. 2020). Ongoing studies are investigating this possibility in the context of protein import clogging.

We then extended our RNA-Seq analysis to other regions within the central nervous system. We selected the striatum and cerebellum for analysis based on the behavioral phenotypes observed in non-paralytic Ant1^{A114P,A123D}/+ mice, namely increased locomotor activity, enhanced balance and coordination, and increased problem-solving. In contrast to spinal cord, we observed minimal transcriptional changes at the individual gene level in the striatum and cerebellum, with only 5 and 28 differentially expressed genes respectively ($q < 0.05$) (Figure S3). The cell type heterogeneity of the striatum likely contributes to the weak signals. Notably absent, though, were any changes in genes involved in oxidative phosphorylation, consistent with a lack of mitochondrial respiratory defects. Instead, pathway analysis revealed global upregulation of proteasomal genes in the striatum (Figure 3C), which would be predicted if protein import clogging is causing mitochondrial Precursor Overaccumulation Stress (mPOS) in the cytosol (*2*, *3*, *14*, *16*). Consistent with disturbed

cytosolic proteostasis, we found that Ubb (ubiquitin B) is the most upregulated gene in the cerebellum (Figure 3D). Ubb transcription was previously shown to be upregulated in neurons of Parkinson's disease patients (*17*). At the protein level, we previously observed upregulation of mono-ubiquitin as well as increased global protein ubiquitination downstream of protein import stress in cultured human cells (*5*). Overall, these transcriptional findings are consistent with extra-mitochondrial proteostasis disruption by mitochondrial protein import clogging.

Different regions of the central nervous system seem to have different stress responses

.

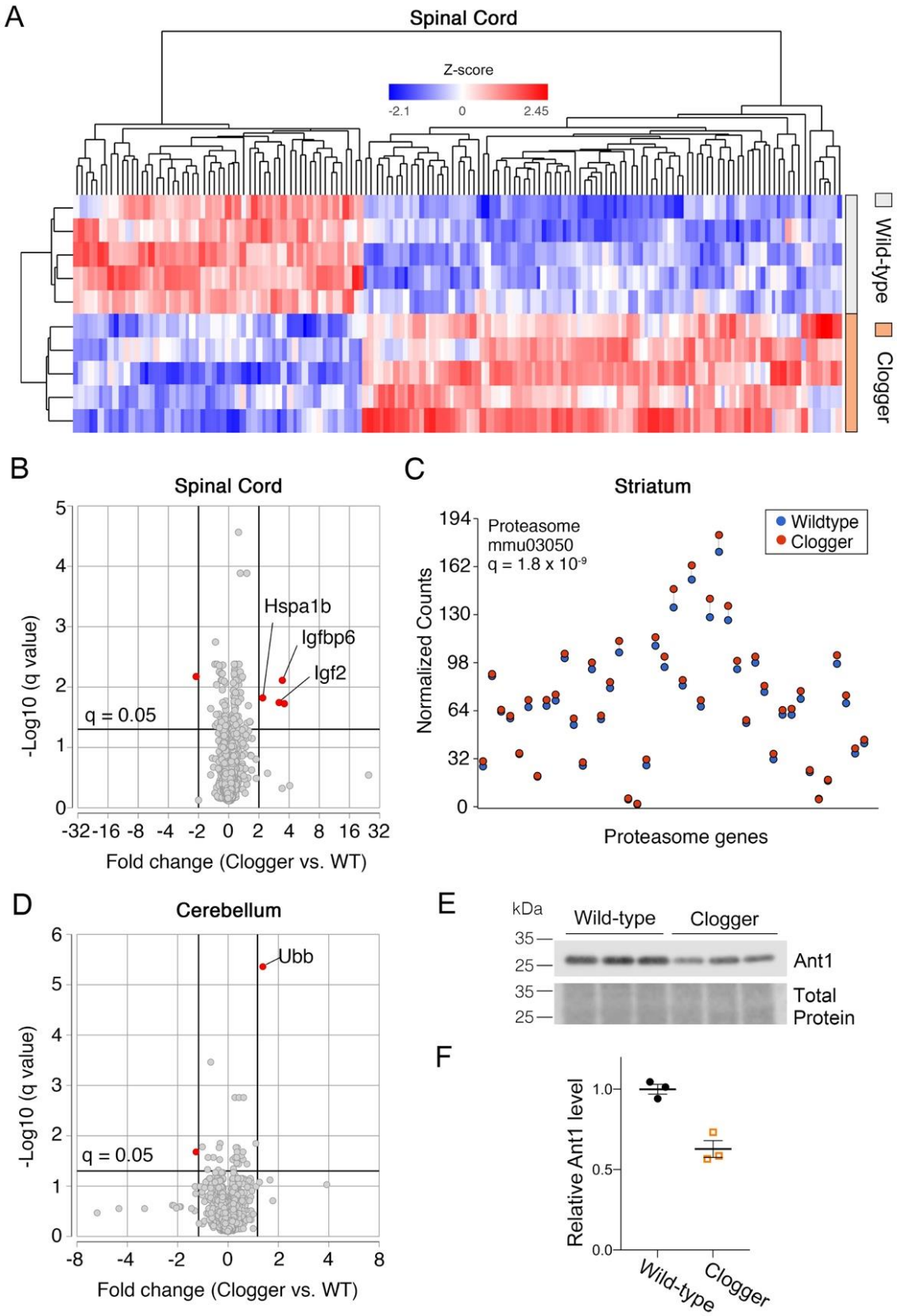

Figure 3. Transcriptomic analysis of neural tissues suggests cytosolic proteostatic stress in the clogger mice.

(A) Heatmap of all genes that are differentially expressed in the spinal cord of clogger mice, compared with wild-type ($q<0.05$).
(B) Partek Pathway analysis of transcriptomics data from the striatum at 24 months of age suggests global proteasome upregulation.
(C) Volcano plot of transcriptomics from the cerebellum at 30 months of age shows significant upregulation of Ubb.
(D) Volcano plot of transcriptomics from the spinal cord at 30 months of age.
(E) Immunoblot showing reduced levels of Ant1 in purified brain mitochondria of clogger mice, presumably due to degradation and/or failed import of the clogger protein, $Ant1^{A114P,A123D}$.
(F) Quantification of data shown in (D), with Ant1 levels normalized by total protein.

Protein import clogging worsens motor deficits, anxiety-like behavior, and modestly reduces maximal lifespan, but does not affect spontaneous locomotor activity or memory in a mouse model of α-synucleinopathy

We speculate that IGF2 upregulation and perhaps additional stress responses are largely sufficient to mitigate neurological dysfunction in non-paralytic clogger mice. Like in skeletal muscle, $Ant1^{A114P,A123D}$ appears to be readily degraded in the brain, as indicated by total Ant1 level being ~60% of wildtype level (Figure 3E-F). Thus, it is still unclear if protein import clogging can contribute to neurodegeneration via cytosolic proteostatic stress. To overcome this, we used mouse genetics to test whether mild protein import stress via $Ant1^{A114P,A123D}$ expression can accelerate cytosolic protein aggregation and disease in an established mouse model of neurodegeneration. We crossed the clogger mice with transgenic mice expressing the human α-synuclein protein with an A53T mutation, which is a dominant cause of familial Parkinson's disease and a highly aggregation-prone cytosolic protein (*18*). A53T α-synuclein (α-syn) mice develop overt neurological dysfunction at 12-16 months of age, which progresses to end-stage

paralysis within 2-3 weeks of symptom onset (*18*). Thus, to detect any effect of Ant1^{A114P,A123D} expression, we characterized the mice at 8-9 months of age. We bred and characterized ~20 mice per sex per genotype.

Motor symptoms are a hallmark of Parkinson's disease. Thus, we assessed balance and coordination using two complementary tasks: beam walking and rotarod analysis. In the beam walking task, mice are trained to walk across a thin beam and the number of times their paws slip off the beam is scored as a measure of coordination (Figure 4A). As expected, α-syn mice slipped more often on both a 0.5-inch diameter cylindrical beam, as well as a 0.25-inch rectangular beam (Figure 4B-C). Ant1^{A114P,A123D} expression drastically enhanced this phenotype on the rectangular beam, while having no effect in the wild-type background. This suggests that Ant1^{A114P,A123D} and α-syn A53T expression act synergistically to impair motor function. As an orthogonal approach to assess motor coordination, we measured the animals' ability to avoid falling off of an accelerating rotarod. In females, Ant1^{A114P,A123D} expression alone improved performance on the rotarod (Figure 4D), consistent with Figure 1A. This effect was abrogated by α-syn A53T expression. In males, α-syn A53T expression alone improved performance on the rotarod, consistent with previous reports (*19*), but Ant1^{A114P,A123D} expression alone did not in this cohort. Increased performance in α-syn mice was abrogated by Ant1^{A114P,A123D} expression. Though complex, these effects are consistent with Ant1^{A114P,A123D} and α-syn A53T expression synergizing to impair motor coordination in mice.

Up to 40% of Parkinson's disease patients experience anxiety (*20*). We found that α-syn expression significantly increased anxiety-like behavior in the open field test, which seemed to be marginally potentiated by Ant1^{A114P,A123D} expression (Figure S4A). While in the center zone, double mutant mice remained closest to the edge zone on average (Figure S4B). Thus,

Ant1^{A114P,A123D} expression moderately increases anxiety-like behavior in α-syn, but not wild-type mice.

We followed these mice through end-stage paralysis to determine if Ant1^{A114P,A123D} expression reduced lifespan in α-syn mice. We found no change in median lifespan in double mutant mice compared with α-syn alone (Figure 4E). Intriguingly, we noticed that the longest-lived double mutant mice died earlier than single mutant α-syn mice. A more detailed analysis of the longest-lived mice showed that maximal lifespan is significantly reduced by Ant1^{A114P,A123D} expression (Figure 4F). In sum, the data show that protein import clogging by Ant1^{A114P,A123D} can accelerate multiple neurological phenotypes and modestly shorten maximum lifespan in a mouse model of cytosolic protein aggregation.

Does protein import clogging aggravate additional phenotypes of α-syn mice? We monitored mouse activity in the open field to test spontaneous locomotor activity. As expected, α-syn mice displayed increased spontaneous locomotor activity (*21*), which was not affected by Ant1^{A114P,A123D} expression (Figure S4C). In the novel object recognition test, α-syn mice showed a significant defect in long-term object memory, with no effect from Ant1^{A114P,A123D} expression (Figure S4D). The total time spent exploring either object was unaffected by genotype (Figure S4E). In the Y-maze spontaneous alternation test, α-syn mice showed a significant defect in short term spatial memory, with no effect of Ant1^{A114P,A123D} expression (Figure S4F). The total number of arm entries in the Y-maze was increased by A53T α-syn expression, with no effect of Ant1^{A114P,A123D} expression (Figure S4G). This is consistent with increased spontaneous locomotor activity of α-syn mice. These data suggest that A53T α-syn impairs memory already

by 9 months old, and that Ant1^{A114P,A123D} expression has no effect in wildtype or α-syn backgrounds.

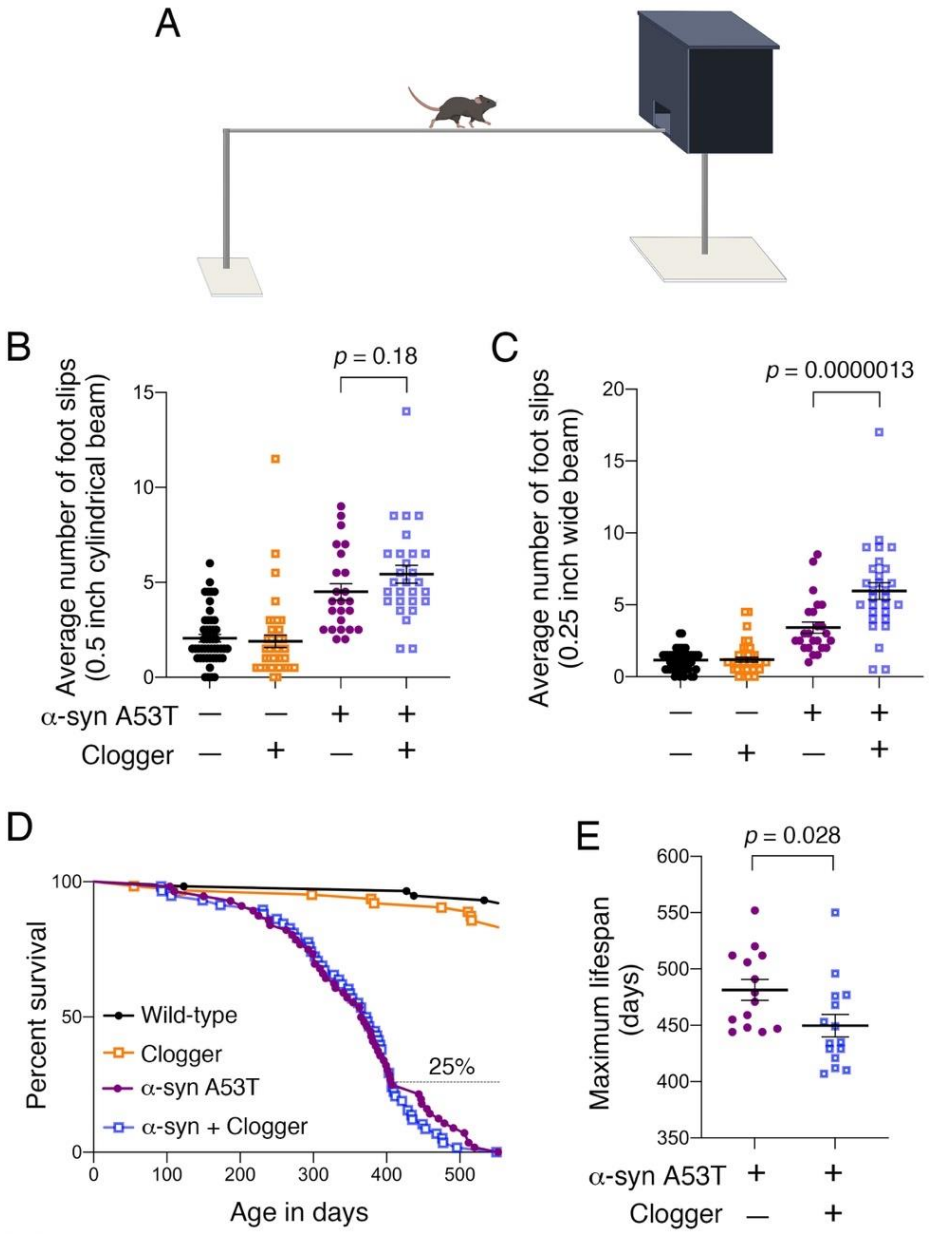

Figure 4. Mild protein import stress disrupts motor coordination only in the α-synuclein^{A53T} transgenic background

(A) Schematic of the beam-walking test.

(B) Beam-walking test suggested mildly worsened coordination on a 0.5-inch cylindrical beam in Ant1$^{A114P, A123D}$ α-Syn A53T double mutant compared with α-Syn A53T single mutant mice, as judged by the number of times each mouse's hind limbs slipped off the

beam. Data were first analyzed with a three-way ANOVA probing for effects of sex, α-synuclien, and clogger genotype. With no significant effect or interaction effect from sex, males and females were consolidated. Adjusted p-value that is shown is from a two-way ANOVA with Sidak's multiple comparison's test.

(C) Beam-walking test suggested severely impaired coordination on a 0.25-inch rectangular beam. Data analyzed as in (B). There was a significant interaction between α-synuclien and clogger genotype ($p = 7.5 \times 10^{-5}$).

(D) Lifespan analysis of at least 56 mice per genotype. The 25% longest-lived mice depicted in (E) are noted on the graph.

(E) Maximum lifespan of the 25% longest-lived mice suggest modestly reduced maximal lifespan in double mutant mice. Data were analyzed by unpaired student's t test.

Ant1$^{A114P, A123D}$-induced import clogging does not affect mitochondrial respiration in α-syn mice.

There are substantial data to suggest that α-syn can impact mitochondrial function, while other studies failed to generate consistent results (*1*). We test the possibility that synergistic defect in mitochondrial function may contribute to the enhanced double mutant phenotypes. We again purified brain mitochondria to measure respiration from complex I and complex II. In our hands, α-syn A53T did not reduce mitochondrial respiratory rates. More importantly, no respiratory defiency was observed even in the Ant1^{A114P,A123D} α-syn double mutant mice (Figure 5A-H). These data suggest that mitochondrial bioenergetic defects are not the cause of motor coordination defects in the α-syn single and Ant1^{A114P,A123D} α-syn double mutant mice.

Because percoll-purified mitochondria are mostly non-synaptosomal, and α-syn primarily localizes to pre-synaptic sites, we also tested respiration from the synaptosomal brain fractions. These fractions are impure, containing microsomal membranes and probably some myelin.

Respiration from synaptosomal fractions also suggested that wild-type, A53T α-syn, and double mutant mice all have similar respiratory rates (Figure S5).

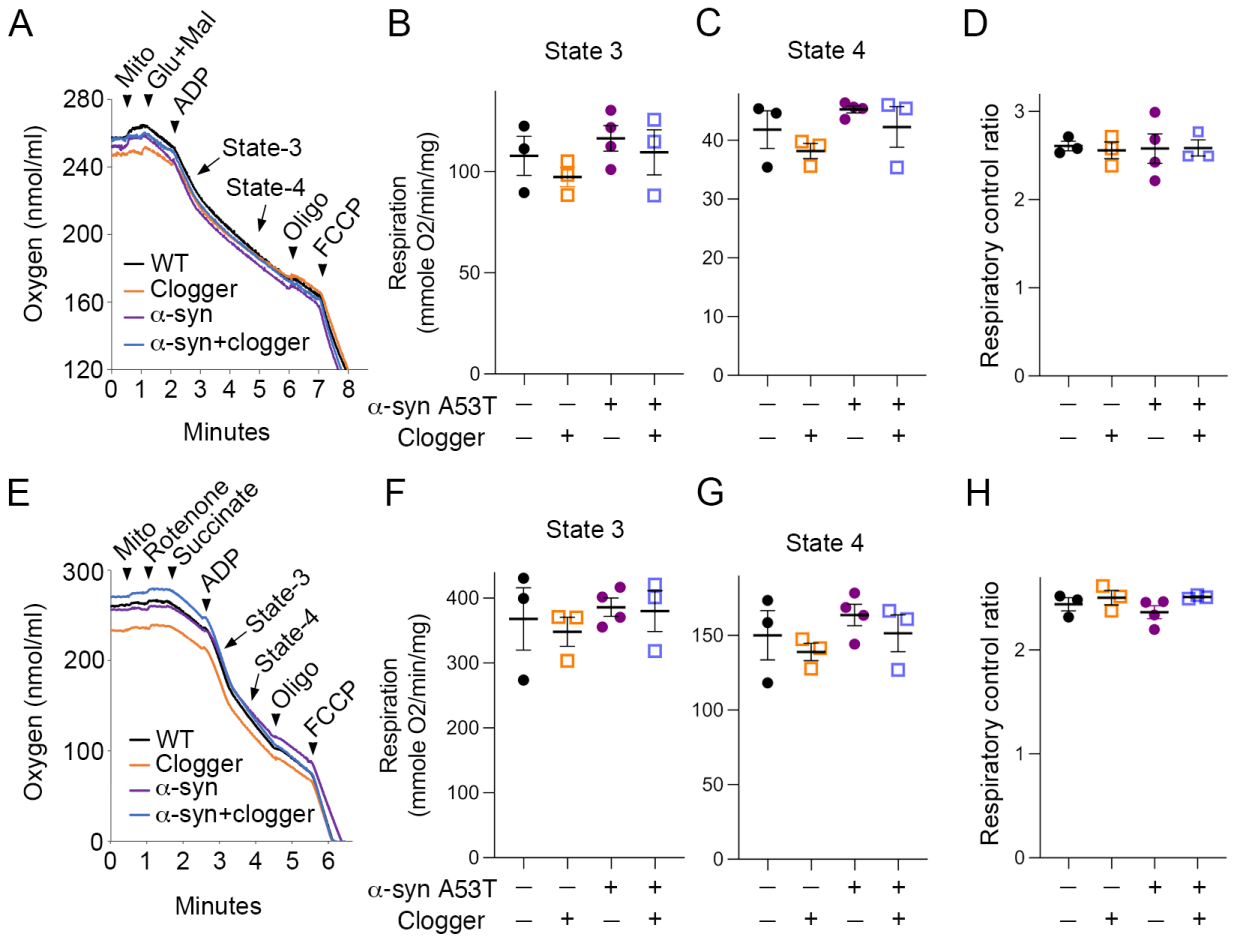

Figure 5. There is no detectable respiratory deficit in 9-month-old α-syn or double mutant mice.

(A) – (D) Respirometry of purified brain mitochondria with complex I stimulated by glutamate (glu) and malate (mal). 2 measurements were taken per mouse, the average of which is shown as a data point in (B)-(D). FCCP, Trifluoromethoxy carbonylcyanide phenylhydrazone; Oligo, oligomycin; Glu, glutamate; Mal, malate. State 3 respiration is the maximal respiratory rate after addition of ADP. State 4 respiration is the respiratory rate after depletion of ADP. The respiratory control ratio is State 3 divided by State 4 respiratory rates. Decreased respiratory control ratio would be interpreted as increased mitochondrial damage. Two measurements per mouse. Each dot represents the average value from each mouse.

(E) – (H) Respirometry of purified brain mitochondria with complex II stimulated by succinate (glu) and complex I inhibited by rotenone. Each dot represents the average value from each mouse.

Discussion

In this report, we provide the foundation for testing a mechanism that can help reconcile two nearly ubiquitous hallmarks across neurodegenerative diseases: mitochondrial dysfunction and cytosolic protein aggregation. We found that mild mitochondrial protein import stress can potentiate neurodegeneration caused by protein misfolding and aggregation in extra-mitochondrial compartments, which seems to be independent of bioenergetics. Specifically, expression of a mutant protein that partially clogs the mitochondrial protein import machinery, Ant1^{A114P,A123D}, worsened motor coordination in pre-paralytic α-synuclein^{A53T} transgenic mice. These findings set the stage for testing whether accumulation of mitochondrial proteins in the cytosol, a process known as mitochondrial Precursor Overaccumulation Stress (mPOS), can contribute to PD-related neurodegeneration through cytosolic protein aggregation.

It has long been appreciated that mitochondrial dysfunction can cause α-synuclein aggregation and PD, but the mechanisms by which this occurs remain unclear. Toxins that inhibit mitochondrial complex I, such as MPTP, cause α-synuclein aggregation and PD in humans and animal models (*22-25*). One consequence of complex I inhibition has been speculated to be mPOS and subsequent α-synuclein aggregation in the cytosol (*3*). Consistent with this, MPTP can reduce protein import in cells as well as *in vitro* (*26*). When protein import is reduced, this has been shown to aggravate seeding of α-synuclein aggregates (*27*). In addition, there is an abundance of circumstantial evidence to suggest that mPOS may contribute to PD independent of direct complex I inhibition. For example, numerous mitochondrial proteins have been found in intra-neuronal protein inclusions in PD mouse models as well as in post-mortem brains from sporadic PD patients (*28-31*). These proteins may indeed represent un-imported mitochondrial preproteins, as mitochondrial protein import may be impaired in PD

brains by direct perturbation by wild-type α-synuclein (*32*), whose expression increases in PD-affected neurons with normal aging (*33*). Similarly, aggregated α-synuclein can reduce mitochondrial membrane potential (*34*), which would be expected to reduce protein import. These observations suggest a model in which an age-dependent increase in α-synuclein level reduces mitochondrial protein import, thereby causing mPOS to aggravate its own aggregation in the cytosol. A similar process may happen in certain forms of familial PD, as loss of PINK1, which is a recessive cause of PD, reduces mitochondrial protein import in mice (*35*). Rigorous evaluation is needed to evaluate the potential contribution of mPOS in PD.

Consistent with defective protein import in PD, analysis of individual nigrostriatal neurons from PD patients showed a large reduction in expression of the nuclear-encoded mitochondrial protein Ndufb8 relative to the mitochondria-encoded COXI protein (*36*). This may reflect reduced import and cytosolic degradation of Ndufb8. Several pathways exist to degrade un-imported preproteins in the cytosol, including proteosome activation via the unfolded protein response activated by mistargeting of proteins (UPRam) (*16, 37*). Transcriptomics of the striatum of clogger mice were consistent with UPRam. The proteasome was also activated in HEK293T cells transfected with a clogger protein (*5*). Which preproteins aggregate versus which are degraded in the cytosol, and why, are important questions for the future.

Whether mitochondrial bioenergetic deficit itself is causative in late-onset neurodegenerative diseases is highly controversial (*38*). For PD, numerous mechanisms by which α-synuclein may directly intoxicate mitochondrial bioenergetics have been proposed (*1*). We were therefore surprised to find no respiratory deficits in synuclein^{A53T} or double mutant mice, despite increased motor symptoms at the same age. Analysis of respiration from purified brain mitochondria actually showed no change in maximal respiratory rate (state 3) in double

mutant mice. The respiratory control ratio, which is considered the single most useful and sensitive general measure of energy coupling efficiency (*39*), was unchanged in the mutant mice. Indeed A53T α-synuclein is expressed in the forebrain of these mice (*18*). These measurements were taken from mice at the same age that motor coordination is severely affected (8-9 months old), strongly arguing that PD-like symptoms can be driven in mice independent of bioenergetics. This is in contrast to previous observations in which COX activity was reduced specifically in the spinal cord of end-stage α-synuclein^{A53T} mice (*40*). It remains possible that COX activity is reduced in the spinal cord of double mutant mice, which could explain the motor defects. To test for this, we collected and frozen mitochondria from the spinal cord, cerebellum, brainstem, as well as synaptosomal fractions of the forebrain of 9-month-old mice. Each of these mitochondrial fractions will be tested for Complex I and COX activity.

Our previous investigation showed that mitochondrial protein import clogging alone challenges cytosolic proteostasis to drive potent cell toxicity (*2, 3, 5*). Interestingly, the majority of clogger mice are able to evade paralytic neurodegeneration and live a normal lifespan. This implies the existence of adaptive mechanisms that mitigate clogging-induced cell stress. One candidate mechanism is degradation of the clogger protein (in this case, Ant1^{A114P,A123D}) which is evident in yeast, human cells, clogger mouse skeletal muscle and brain (Fig. 3E-F). How such degradation occurs is unclear, though "de-clogging" processes have been elegantly identified in yeast (*41, 42*). Another candidate mechanism is upregulation of IGF-2, as detected in the spinal cord of non-paralytic clogger mice. This finding was of particular interest because spinal cord degeneration is prominent in paralytic clogger mice. IGF-2 has emerged in recent years as a neuroprotective protein in several neurodegenerative diseases with prominent protein aggregation and mitochondrial dysfunction (*43-45*). Mechanistically, this seems to occur

through the extracellular disposal of cytosolic protein aggregates (*45*). Taken together, it appears that neurons possess intrinsic pathways to mitigate the effects of moderate mitochondrial protein import clogging. At this severity of protein import stress, a "second hit" to cytosolic proteostasis may be required for negative effects on neurological function, as suggested by double mutant clogger plus α-syn mice.

One intriguing finding of our study is the apparently better-functioning neurological attributes in non-paralytic clogger mice. These mice perform better than wildtype mice on the rotarod and in the puzzle box assay, both of which could be explained by improved executive function. Similar observations have been observed downstream of mitochondrial damage that causes respiratory deficiency (*12*). Respiratory deficiency is absent in clogger mice, suggesting that it is not a prerequisite for improved executive function. Mild mitochondrial dysfunction improving organismal fitness is known as mitohormesis, and is well documented across model systems (*46*). Future work is required to investigate the mechanism of this apparent mitohormetic response to protein import clogging.

In summary, we utilized non-paralytic clogger mice to study the neurological effects of mild mitochondrial protein import stress in both healthy and diseased conditions. We found that mild import stress can readily be mitigated in otherwise healthy mice. Upregulation of IGF-2 and extracellular disposal of protein aggregates. In a mouse model of PD expressing mutant α-synuclein, mild import stress potentiates neurodegeneration. Preliminary findings suggest this occcurs independent of bioenergetics. Thus, protein import efficiency appears to be a disease modifying factor in PD independent of OXPHOS.

Limitations of Study

The primary objective of this study is to determine whether moderate protein import stress can potentiate neurodegeneration by increasing protein misfolding and aggregation in the cytosol via mPOS. Our study therefore remains incomplete. Histological analysis and detergent solubility studies will be important in testing whether Ant1^{A114P,A123D} accelerates and/or increases α-syn-induced aggregate formation *in vivo*. It would also be interesting to know whether mitochondrial proteins co-aggregate with α-synuclien in these mice, and whether this is increased by protein import stress, as previously shown in yeast (*47*).

In addition, more experiments are required to definitively rule out bioenergetic defects as the cause of α-syn and/or double mutant mouse phenotypes at 8-9 months of age. Aside from the brain, it was previously reported that cytochrome C oxidase activity is specifically reduced in the spinal cord of end-stage α-synucline^{A53T} mice (*40*). This finding may or may not be relevant to pathophysiology, as such a reduction would be expected with widespread cell death that likely occurs in the spinal cord of paralyzed mice. Nevertheless, we will test respiratory enzyme activity from mitochondria-enriched fractions from the spinal cord, cerebellum, and brainstem.

Methods

Mouse studies

All procedures were approved by the Animal Care and Use Committee (IACUC) at State University of New York Upstate Medical University and were in accordance with guidelines established by the National Institutes of Health. Ant1^{A114P,A123D}/+ mice, or "clogger" mice, were generate as previously described (Coyne et al., 2022, *submitted*). After >10 back crosses with the C57BL/6NTac females (Taconic Catalog no: B6-F), male Ant1^{A114P,A123D}/+ mice were crossed with female C57BL/6 mice with transgenic expression of the human *SNCA* gene (coding for the α-synuclein protein) harboring the pathogenic A53T mutation (Jackson Lab #006823) (*18*). *SNCA* expression is driven by the mouse prion promoter in these mice. Where α-syn mice were tested, all wild-type and clogger control mice were littermates.

Mitochondrial isolation and purification

For mitochondrial respiratory studies, mice were sacrificed by decapitation without CO_2 asphyxiation or anesthetic. Neural tissues were rapidly dissected (<60 seconds) and placed in 1 mL of ice-cold Isolation Medium (IM) (225 mM Mannitol, 75 mM sucrose, 5 mM HEPES-KOH pH 7.4, 1 mM EGTA, 0.1% BSA). Quick dissection of the spinal cord was enabled via hydraulic extrusion with ice-cold PBS (*48*). Tissue was minced on ice while submerged in IM as soon as possible. For crude mitochondrial fraction isolation (i.e. for crebellum, spinal cord, and brain stem), well-minced tissue was homogenized with 4 strokes by hand in a 2 mL glass dounce homogizer (pestle B, clearance 0.0005-0.0025 inches), followed by differential centrifugation at 4^{o}C. First, homogenate was centrifuged at 2,000g for 5 minutes. Supernatant was then centrifuged at ~21,000g for 20 minutes. Pellet was resuspended in 0.5 mL IM and centrifuged

again at ~21,000g for 20 minutes. Again, pellet was resuspended in 0.5 mL IM and centrifuged again at ~21,000g for 20 minutes. The final pellet was resuspended in 0.2 mL IM.

Mitochondria were purified from the forebrain, which in our studies includes all neural tissue anterior to the junction between the cerebral cortex and the cerebellum. This was done essentially as previously described (*49*). For purification, minced forebrains were homogenized with three strokes with the pestle at 13,900 rpm in ice cold 7 mL IM. Homogenate was then centrifuged for 5 minutes at 2,000g. Resulting supernatant was centrifguged at 13,000 g for 12 minutes. Pellet was then resuspended in 2 mL IM containing 12% percoll, and used to build a discontinuous gradient using the following percoll concentrations in isotonic IM: 5 mL 40%, 5 mL 23%, and ~2.5 mL 12% (mito). Gradients were ultra-centrifuged in a swinging-bucket rotor (SW 41) at 18,500 rpm (~43,000 g) for 20 minutes with slow acceleration and deceleration. Purified non-synaptosomal mitochondria were retrieved from the 23/40% interface, and synaptosomes were collected from the 23/12% interface. Both fractions were then diluted with ~25 mL IM without percoll, and centrifuged at 13,000g for 15 minutes. Mitochondrial pellet was resuspended in 1 mL IM and centrifuged at 13,000g for 12 minutes. Mitochondria were then washed two more times in 1 mL ice-cold IM, and finally resuspended in 80 µl for non-synpatosomal pure mitochondria, and 200 µl for synaptosomes. Protein concentration was then determined by Brandford assay.

Mitochondrial oxygen consumption measurements

Oxygen consumption assays were performed using Oxygraph system form Hansatech, which has a small water-jacketed (37^{o}C), magnetically-stirred chamber sitting atop a Clark

electrode. Each reaction occurred in 0.5 ml Respiratory buffer (125 mM KCl, 4 mM K_2HPO_4, 3 mM $MgCl_2$, 1 mM EGTA, 20 mM HEPES-KOH pH 7.2). 150 μg or 300 μg of non-synaptosomal and synaptosomal mitochondria, respectively, were added first. Then, for Complex I-based respiration, reagents were added in the following sequence at the indicated final concentrations: Glutamate (5 mM) + Malate (2.5 mM); ADP (200 μM); oligomycin (3 μg/ml); FCCP (0.2 μM). For Complex II: rotenone (5 μM); succinate (10μM); ADP (300 μM); oligomycin (3 μg/ml); FCCP (0.2 μM).

Electron microscopy

For electron microscopy, $Ant1^{A114P,A123D/+}$ mice and littermate controls were processed as previously described (*50*). Briefly, mice were anesthetized with isoflurane and perfused intracardially with PBS initially, followed by fixative (1% paraformaldehyde, 1% glutaraldehyde, 0.12 M sodium cacodylate buffer pH 7.1, and 1 mM $CaCl_2$). Perfused animals were refrigerated overnight and CNS tissues dissected the next day and processed for TEM. The samples were examined with a JOEL JEM1400 transmission electron microscope and images were acquired with a Gaten DAT-832 Orius camera.

Immunoblot analysis

Purified brain mitochondria were solubilized in Laemmli buffer and processed for Western blotting using standard procedures and Total OXPHOS Antibody Cocktail (#ab110411, Abcam).

RNA sequencing & analysis

Neural tissues were dissected and snap-frozen as quickly as possible, and the spinal cord ejected from the spinal canal via hydraulic extrusion with ice cold DEPC-treated PBS. Accurate identification of the striatum was less straight forward than the cerebellum and spinal cord. First, cerebellar, brain stem, and olfactory bulb were removed from the forebrain. The brain was then cut sagittally along the interhemispheric fissure. Approaching from the medial aspect of the brain, inner brain material (including the thalamus, septum and underlying striatum) was removed by cutting just below the corpus collosum, thus separating these tissues from the hippocampus and associated cerebral cortex. The easily-identifiable thalamus and hypothalamus were removed, and the remaining tissue from this "inner brain" material was labeled striatum. Tissue was frozen in liquid nitrogen.

Behavioral Assays

Behavioral assays were performed in a particular order to minimize the likelihood that one test affects mouse behavior on subsequent days. The order went as follows: elevated plus maze, Y-maze spontaneous alternation test, open field activity test, novel object recognition test, Morris Water Maze, puzzle box test, followed by prepulse inhibition test. Male and female mice were tested in all assays. Each data point shown in Figure S5 represents an independent mouse. Elevated plus maze, y-maze spontaneous alternation, and open field activity testing were done on two independent cohorts. For every test, mice were habituated to the testing room for 30 minutes prior to each test, and odors and residue was removed after each test with 70% ethanol. Mouse

activity and scoring in each test was automatically measured using ANY-Maze behavioral tracking software, except for puzzle box testing, which was scored manually, and prepulse inhibition test, which was scored using Startle-Pro software (Med Associates, Fairfax, VT). Elevated plus maze, y-maze, open field activity, novel object recognition and prepulse inhibition testing was done as previously described (*51*).

Elevated plus maze (EPM)

EPM is used to assess anxiety-like behavior. We used a standard mouse EPM apparatus from San Diego Instruments, which consists of two closed arms and two open arms perpendicular to one another, forming a "plus" shape. Mice were placed in the center of the apparatus, facing an open arm, and allowed to explore freely for 5 minutes under ambient light. The time spent in the open arms is reported to reflect anxiety-like behavior, such that the less time in the open arms, the more anxiety-like the behavior is.

Y-maze Spontaneous Alternation Test

We used the Y-maze Spontaneous Alternation Test to assess spatial working memory. A custom-built apparatus was used, which consisted of 3 walled arms 16 inches long that are angled 120^{o} from one another. Mice were placed in the center and allowed to freely explore for 5 minutes in dim light. This test is based on the rodent's tendency to explore new environments. Exploring the 3 arms consecutively, without re-entry into an arm, is called a triad. This implies that the mouse "remembers" which arm it was most recently in, despite all arms appearing identical. To control for difference in total number of arm entries, we report Fraction of

Alternation, which is (total number of triads) / (total number of arm entries – 2). Mice with less than 5 total arm entries were excluded from Fraction of Alternation analysis.

Open field activity test

Open field activity testing was performed to assess spontaneous locomotor activity and anxiety-like behavior. We used a standard apparatus from San Diego Instruments, which consists of 50 cm x 50 cm open field surrounded by non-transparent walls. Mice were allowed to explore freely for 10 minutes in ambient light. Time spent in a pre-designated "center zone" is reported to reflect anxiety-like behavior, such that the less time spent in the center, the more anxiety-like the behavior is.

Novel object recognition (NOR) test

NOR testing was performed to assess long-term object recognition memory and was performed in the open field apparatus. Briefly, two identical objects (cubes) were placed in the chamber and the mice were allowed to explore the objects for 5 minutes per day in dim lighting for two training days. On the third day, a novel object (cylindrical piece of wood) replaced one of the cubes, and mice were allowed to explore the chamber for 10 minutes. If the mice remember the objects from the training days, then they have a tendency to spend more time exploring the novel object. Reported is the time spent interacting with the novel object on the final day of testing. Mice with less than 5 seconds of total object exploration time on the final testing day were excluded from discrimination index analysis.

Morris water maze

Morris water maze was performed to assess long-term spatial memory and learning, and was performed in an inflatable hot tub with the water temperature at 26^{o}C in dim lighting, essentially as previously described (*52*). Briefly, mice were placed in the circular pool for 4 trials per day and allowed one minute to find a platform that they can stand on. Platform was made of transparent plastic and placed just beneath the water surface as to make it invisible to the rodents. For pre-training day 1, mice were placed on the platform for one minute, followed by placement of the mouse proximally to the platform so it learns it can escape the water. On pre-training day 2, mice were placed in a pseudo-randomized quadrant of the pool and allowed one minute to escape to the platform, which was made visible on this day with a small flag. Then, for 7 training days, the platform was below the surface with no flag, and the mice were given 4 trials per day to learn where the platform was using spatial cues from around the room. On the probe day, the day after training day 7, the platform was removed, and the amount of time the mice spent swimming in the quadrant of the pool that previously had the platform, as well as the number of times the mice entered the platform zone, were recorded. The better long-term spatial memory the rodent has, the more time it spends in the target quadrant, and the more times it will enter the platform zone.

Puzzle Box Test

To assess executive function, we performed the puzzle box test as previously described (*9, 10*). Briefly, mice were placed in a custom-built 60 cm x 28 cm apparatus that is well-lit with a small fan blowing into it to create a stressful environment. The mice are given a passage (5 cm by 5 cm doorway) to small and dark target location filled with home bedding to make the mice comfortable. The idea is to test the mouse's ability to "problem solve" by removing obstacles

between the stressful environment and the target location. Condition 0, there is no obstacle. Condition 1 had a U-shaped channel within the doorway. Condition 2 had the same U-shaped channel within the doorway, but with a mound of cage bedding placed in it to block the doorway. Condition 3 had a crumped piece of paper placed in the door way. Finally, condition 4 had a cube placed in the door way, with a raised edge on top of it such that the mice had to pull it out of the doorway and could not push it through. We manually recorded the time it took to reach the target location, and plotted that as "escape latency". Maximum of 5 minutes seconds was allowed.

Beam walking test

Beam walking test was used as a measure of balance and coordination. Although typically the primary read-out for this assay is time to traverse the beam, analysis of these data were compromised by the substantially increased locomotor activity of transgenic α-synuclein^{A53T} mice. Thus, we prioritized the number of times each mouse's hind limbs slipped off of the beam as the primary read-out for balance and coordination.

We custom-built a beam walking apparatus, consisting of a one-meter-long wooden beam ~16 inches suspended above the ground. The start end of the beam was suspended in the air without an escape route, and the other end has the target box for the mice to escape into. The target box is an enclosed black cube of about 9 inches on each side. Before each test, home bedding from the tested mouse is added to the escape box for enticement. Aversive stimuli (a bright LED light and a small fan) were placed at the start end of the beam such that the escape box was the only route to protection. Mice were trained on an easy beam (0.5-inch rectangle) over two days. In training, if a mouse stopped moving while on the beam it was prodded by the

experimenter. On training day 1, the mouse was placed directly in the target box for one minute, then placed on the beam two inches from the target box and allowed to escape to the target box, and finally placed at the far end of the beam for full traverse of the beam. On training day 2, each mouse was given 3 more trials on the easy beam. On test day, each mouse was tested twice on 0.5-inch circular and 0.25-inch rectangular beams. The number of hind limb slips per beam was manually scored by an experimenter who was blinded to genotype. Plotted in Figure 5 is the average number of slips of the two trials.

Treadmill exhaustion test

Treadmill tests were performed on an Exer 3/6 animal treadmill at a 5^{o} incline (Columbus Instruments). For one week, mice were familiarized with the treadmill with 10-minute running sessions at 10 m/min every other day. For resistance testing, the treadmill started at 9 m/min with 1.2 m/min/min acceleration until the mice reached exhaustion. For power testing, the treadmill started at 9 m/min with 1.8 m/min/min acceleration until the mice reached exhaustion. Mice were deemed exhausted when they remained in continuous contact with the shock grid for 5 seconds. Three full days of rest were allowed between training and each testing day.

Optomotor response test

Optomotor acuity and contrast sensitivity of mice were determined by observing their optomotor behavior responses to a rotating sine wave grating stimulus using the OptoMotry© system (*53*) as described previously (*54, 55*). Briefly, mice were placed on a pedestal at a center of the OptoMotry chamber enclosed by four computer monitors. The computer randomly displayed sinusoidal pattern gratings rotating in a clockwise or counter-clockwise direction. The

observer was blind to the direction of rotation and chose the direction of pattern rotation based on the animal's behavior. Auditory feedback indicated to the observer whether the selected direction was correct or incorrect. Using a staircase paradigm, the computer program controlled the spatial frequency and contrast of the stimulus. The threshold was set at 70% correct responses. Contrast sensitivity was defined as the reciprocal of the threshold contrast value and was measured at 1.5 Hz and a spatial frequency of 0.128 cycles/degree. Acuity was measured at a speed of rotation of 12 degrees/s and 100% contrast. All measurements were performed at the unattenuated maximal luminance of the OptoMotry© system (~70 cd/m^2, producing approximately 1500 R*/rod/s (*56*)).

4.6.15 – Statistical Analysis

Statistical analyses were performed using either GraphPad Prism or SPSS software. For behavioral tests, we always probed for a statistically significant effect of Genotype, Sex and Genotype x Sex interactions. If data are presented without separating sex, this indicates there was no significant main effect of sex and that there was no significant Genotype x Sex interaction. For details on statistical testing of specific data, please see Figure Legends.

References:

1. H. Kawamata, G. Manfredi, Proteinopathies and OXPHOS dysfunction in neurodegenerative diseases. *J Cell Biol* **216**, 3917-3929 (2017).
2. X. Wang, X. J. Chen, A cytosolic network suppressing mitochondria-mediated proteostatic stress and cell death. *Nature* **524**, 481-484 (2015).
3. L. P. Coyne, X. J. Chen, mPOS is a novel mitochondrial trigger of cell death - implications for neurodegeneration. *FEBS Lett* **592**, 759-775 (2018).
4. W. Liu, X. Duan, X. Fang, W. Shang, C. Tong, Mitochondrial protein import regulates cytosolic protein homeostasis and neuronal integrity. *Autophagy* **14**, 1293-1309 (2018).
5. Y. Liu *et al.*, Mitochondrial carrier protein overloading and misfolding induce aggresomes and proteostatic adaptations in the cytosol. *Mol Biol Cell* **30**, 1272-1284 (2019).
6. W. Neupert, J. M. Herrmann, Translocation of proteins into mitochondria. *Annu Rev Biochem* **76**, 723-749 (2007).
7. T. Endo, K. Yamano, Multiple pathways for mitochondrial protein traffic. *Biol Chem* **390**, 723-730 (2009).
8. N. Wiedemann, N. Pfanner, Mitochondrial Machineries for Protein Import and Assembly. *Annu Rev Biochem* **86**, 685-714 (2017).
9. N. M. Ben Abdallah *et al.*, The puzzle box as a simple and efficient behavioral test for exploring impairments of general cognition and executive functions in mouse models of schizophrenia. *Exp Neurol* **227**, 42-52 (2011).
10. A. M. O'Connor, T. J. Burton, C. A. Leamey, A. Sawatari, The use of the puzzle box as a means of assessing the efficacy of environmental enrichment. *J Vis Exp*, (2014).

11. H. Tyynismaa *et al.*, Mutant mitochondrial helicase Twinkle causes multiple mtDNA deletions and a late-onset mitochondrial disease in mice. *Proc Natl Acad Sci U S A* **102**, 17687-17692 (2005).

12. T. L. Emmerzaal *et al.*, Impaired mitochondrial complex I function as a candidate driver in the biological stress response and a concomitant stress-induced brain metabolic reprogramming in male mice. *Transl Psychiatry* **10**, 176 (2020).

13. J. C. Young, N. J. Hoogenraad, F. U. Hartl, Molecular chaperones Hsp90 and Hsp70 deliver preproteins to the mitochondrial import receptor Tom70. *Cell* **112**, 41-50 (2003).

14. F. Boos *et al.*, Mitochondrial protein-induced stress triggers a global adaptive transcriptional programme. *Nat Cell Biol* **21**, 442-451 (2019).

15. L. A. Bach, Insulin-like growth factor binding protein-6: the "forgotten" binding protein? *Horm Metab Res* **31**, 226-234 (1999).

16. L. Wrobel *et al.*, Mistargeted mitochondrial proteins activate a proteostatic response in the cytosol. *Nature* **524**, 485-488 (2015).

17. J. M. Kim *et al.*, Identification of genes related to Parkinson's disease using expressed sequence tags. *DNA Res* **13**, 275-286 (2006).

18. M. K. Lee *et al.*, Human alpha-synuclein-harboring familial Parkinson's disease-linked Ala-53 --> Thr mutation causes neurodegenerative disease with alpha-synuclein aggregation in transgenic mice. *Proc Natl Acad Sci U S A* **99**, 8968-8973 (2002).

19. P. S. Guerreiro *et al.*, Mutant A53T alpha-Synuclein Improves Rotarod Performance Before Motor Deficits and Affects Metabolic Pathways. *Neuromolecular Med* **19**, 113-121 (2017).

20. K. Walsh, G. Bennett, Parkinson's disease and anxiety. *Postgrad Med J* **77**, 89-93 (2001).

21. E. L. Unger *et al.*, Locomotor hyperactivity and alterations in dopamine neurotransmission are associated with overexpression of A53T mutant human alpha-synuclein in mice. *Neurobiol Dis* **21**, 431-443 (2006).

22. G. C. Davis *et al.*, Chronic Parkinsonism secondary to intravenous injection of meperidine analogues. *Psychiatry Res* **1**, 249-254 (1979).

23. J. W. Langston, P. Ballard, J. W. Tetrud, I. Irwin, Chronic Parkinsonism in humans due to a product of meperidine-analog synthesis. *Science* **219**, 979-980 (1983).

24. R. S. Burns *et al.*, A primate model of parkinsonism: selective destruction of dopaminergic neurons in the pars compacta of the substantia nigra by N-methyl-4-phenyl-1,2,3,6-tetrahydropyridine. *Proc Natl Acad Sci U S A* **80**, 4546-4550 (1983).

25. R. Betarbet *et al.*, Chronic systemic pesticide exposure reproduces features of Parkinson's disease. *Nat Neurosci* **3**, 1301-1306 (2000).

26. S. Franco-Iborra *et al.*, Defective mitochondrial protein import contributes to complex I-induced mitochondrial dysfunction and neurodegeneration in Parkinson's disease. *Cell Death Dis* **9**, 1122 (2018).

27. J. Lautenschlager *et al.*, Intramitochondrial proteostasis is directly coupled to alpha-synuclein and amyloid beta1-42 pathologies. *J Biol Chem* **295**, 10138-10152 (2020).

28. M. Hashimoto, A. Takeda, L. J. Hsu, T. Takenouchi, E. Masliah, Role of cytochrome c as a stimulator of alpha-synuclein aggregation in Lewy body disease. *J Biol Chem* **274**, 28849-28852 (1999).

29. S. Gandhi *et al.*, PINK1 protein in normal human brain and Parkinson's disease. *Brain* **129**, 1720-1731 (2006).

30. J. B. Leverenz *et al.*, Proteomic identification of novel proteins in cortical lewy bodies. *Brain Pathol* **17**, 139-145 (2007).

31. L. Chen, Z. Xie, S. Turkson, X. Zhuang, A53T human alpha-synuclein overexpression in transgenic mice induces pervasive mitochondria macroautophagy defects preceding dopamine neuron degeneration. *J Neurosci* **35**, 890-905 (2015).

32. R. Di Maio *et al.*, alpha-Synuclein binds to TOM20 and inhibits mitochondrial protein import in Parkinson's disease. *Sci Transl Med* **8**, 342ra378 (2016).

33. Y. Chu, J. H. Kordower, Age-associated increases of alpha-synuclein in monkeys and humans are associated with nigrostriatal dopamine depletion: Is this the target for Parkinson's disease? *Neurobiol Dis* **25**, 134-149 (2007).

34. A. K. Reeve *et al.*, Aggregated alpha-synuclein and complex I deficiency: exploration of their relationship in differentiated neurons. *Cell Death Dis* **6**, e1820 (2015).

35. S. Gispert *et al.*, Parkinson phenotype in aged PINK1-deficient mice is accompanied by progressive mitochondrial dysfunction in absence of neurodegeneration. *PLoS One* **4**, e5777 (2009).

36. A. Grunewald *et al.*, Quantitative quadruple-label immunofluorescence of mitochondrial and cytoplasmic proteins in single neurons from human midbrain tissue. *J Neurosci Methods* **232**, 143-149 (2014).

37. J. Song, J. M. Herrmann, T. Becker, Quality control of the mitochondrial proteome. *Nat Rev Mol Cell Biol* **22**, 54-70 (2021).

38. E. Area-Gomez, C. Guardia-Laguarta, E. A. Schon, S. Przedborski, Mitochondria, OxPhos, and neurodegeneration: cells are not just running out of gas. *J Clin Invest* **129**, 34-45 (2019).

39. M. D. Brand, D. G. Nicholls, Assessing mitochondrial dysfunction in cells. *Biochem J* **435**, 297-312 (2011).

40. L. J. Martin *et al.*, Parkinson's disease alpha-synuclein transgenic mice develop neuronal mitochondrial degeneration and cell death. *J Neurosci* **26**, 41-50 (2006).

41. H. Weidberg, A. Amon, MitoCPR-A surveillance pathway that protects mitochondria in response to protein import stress. *Science* **360**, (2018).

42. C. U. Martensson *et al.*, Mitochondrial protein translocation-associated degradation. *Nature* **569**, 679-683 (2019).

43. T. J. Mellott, S. M. Pender, R. M. Burke, E. A. Langley, J. K. Blusztajn, IGF2 ameliorates amyloidosis, increases cholinergic marker expression and raises BMP9 and neurotrophin levels in the hippocampus of the APPswePS1dE9 Alzheimer's disease model mice. *PLoS One* **9**, e94287 (2014).

44. I. Allodi *et al.*, Differential neuronal vulnerability identifies IGF-2 as a protective factor in ALS. *Sci Rep* **6**, 25960 (2016).

45. P. Garcia-Huerta *et al.*, Insulin-like growth factor 2 (IGF2) protects against Huntington's disease through the extracellular disposal of protein aggregates. *Acta Neuropathol* **140**, 737-764 (2020).

46. J. Yun, T. Finkel, Mitohormesis. *Cell Metab* **19**, 757-766 (2014).

47. U. Nowicka *et al.*, Cytosolic aggregation of mitochondrial proteins disrupts cellular homeostasis by stimulating the aggregation of other proteins. *Elife* **10**, (2021).

48. M. Richner, S. B. Jager, P. Siupka, C. B. Vaegter, Hydraulic Extrusion of the Spinal Cord and Isolation of Dorsal Root Ganglia in Rodents. *J Vis Exp*, (2017).

49. T. Kristian, Isolation of mitochondria from the CNS. *Curr Protoc Neurosci* **Chapter 7**, Unit 7 22 (2010).

50. P. T. Massa, C. Wu, K. Fecenko-Tacka, Dysmyelination and reduced myelin basic protein gene expression by oligodendrocytes of SHP-1-deficient mice. *J Neurosci Res* **77**, 15-25 (2004).

51. P. Afshari, W. D. Yao, F. A. Middleton, Reduced Slc1a1 expression is associated with neuroinflammation and impaired sensorimotor gating and cognitive performance in mice: Implications for schizophrenia. *PLoS One* **12**, e0183854 (2017).

52. C. V. Vorhees, M. T. Williams, Morris water maze: procedures for assessing spatial and related forms of learning and memory. *Nat Protoc* **1**, 848-858 (2006).

53. G. T. Prusky, N. M. Alam, S. Beekman, R. M. Douglas, Rapid quantification of adult and developing mouse spatial vision using a virtual optomotor system. *Invest Ophthalmol Vis Sci* **45**, 4611-4616 (2004).

54. Y. Umino *et al.*, Hypoglycemia leads to age-related loss of vision. *Proc Natl Acad Sci U S A* **103**, 19541-19545 (2006).

55. Y. Umino, E. Solessio, R. B. Barlow, Speed, spatial, and temporal tuning of rod and cone vision in mouse. *J Neurosci* **28**, 189-198 (2008).

56. M. Bushnell, Y. Umino, E. Solessio, A system to measure the pupil response to steady lights in freely behaving mice. *J Neurosci Methods* **273**, 74-85 (2016).